USGS Award No. 08HQGR0024

APPLICATION OF PROBABILISTIC METHODS FOR MAPPING EARTHQUAKE-INDUCED LANDSLIDE POTENTIAL

FINAL TECHNICAL REPORT

SUBMITTED: 4 May 2009

Ellen M. Rathje, Ph.D., P.E.
University of Texas at Austin
ECJ 9.227, C1792
Austin, TX 78712
Tel: 512-471-4929
Fax: 512-471-6548
e.rathje@mail.utexas.edu
http://www.caee.utexas.edu/dept/area/geotech/GeotechnicalEngr.htm

NEHRP Element: I
Key Words: seismic landslide maps, probabilistic approach, sliding block analysis

Research supported by the U.S. Geological Survey (USGS), Department of the Interior, under USGS award number (08HQGR0024). The views and conclusions contained in this document are those of the authors and should not be interpreted as necessarily representing the official policies, either expressed or implied, of the U.S. Government

ABSTRACT

Seismic landslide hazard maps are used to identify zones with a significant risk of earthquake-induced landslides. These maps are based on predicted levels of rigid sliding block displacement for given ground motion and yield acceleration conditions. This paper presents a probabilistic methodology to develop seismic landslide hazard maps. This approach is an improvement over current approaches because it considers both the uncertainties in the ground motion prediction and the prediction of sliding displacement. The probabilistic approach computes the annual rate of exceedance for different levels of sliding displacement given the yield acceleration of a slope and a probabilistic description of the ground motion. The displacement level with a 10% probability of exceedance in 50 years is used to identify landslide hazard zones. A scalar approach, which uses peak ground acceleration and earthquake magnitude to predict sliding displacement, and a vector approach, which uses peak ground acceleration and peak ground velocity to predict sliding displacement, are used in this work. The probabilistic methodologies are applied to the Mint Canyon Quadrangle in Southern California to develop seismic landslide hazard maps. These maps indicate that the scalar probabilistic methodology produces slightly larger seismic landslide hazard zones than current methodologies because it incorporates the displacement prediction uncertainty. However, the vector probabilistic approach significantly reduces the size of the seismic landslide hazard zones because of the additional information provided by the multiple ground motion parameters.

NON-TECHNICAL SUMMARY

Seismic landslide hazard maps are used to identify zones with a significant risk of earthquake-induced landslides, and they help guide decisions regarding infrastructure development and they provide the impetus for more detailed studies for proposed developments. This report describes probabilistic methodologies for developing seismic landslide maps. These maps deal with the important uncertainties related to predicting ground shaking and to predicting sliding displacements. The probabilistic methodologies are applied to a quadrangle in Southern California and the resulting maps compared to those prepared using current approaches.

INTRODUCTION

Recent earthquakes, such as the 2008 Wenchuan, China earthquake, have demonstrated that earthquake-induced landslides are a significant seismic hazard. Seismic landslide hazard maps have been developed throughout seismically active areas to identify zones where the risk of earthquake-induced landslides is high. Additionally, since the early 1990's, the Seismic Hazards Mapping Act of California has required that the California Geological Survey (CGS) develop seismic hazard zone maps for various seismic hazards, including liquefaction, strong ground shaking, and landslides. These seismic hazard zone maps help guide decisions regarding infrastructure development and provide the impetus for more detailed studies for proposed developments.

Seismic landslide hazard mapping is based on predicting rigid sliding block displacements at discrete locations over a regional area (e.g., Jibson et al. 2000, McCrink 2001). The rigid sliding block approach represents a slope as a frictional block sliding down an inclined plane (Figure 1a). The yield acceleration (k_y) of the sliding block represents the horizontal acceleration that results in a factor of safety equal to 1.0 for the slope and this acceleration level initiates sliding. The yield acceleration can be derived using an infinite slope model (Figure 1b) and is a function of multiple slope characteristics, including the slope angle, shear strength parameters, and ground water conditions. For a given earthquake acceleration-time history ($a(t)$), the slope becomes unstable when the acceleration exceeds k_y. At this point, a sliding episode begins and permanent, downslope displacements occur. A sliding episode continues until the relative sliding velocity between the block and ground is zero. The sliding displacement is calculated from double integration of the relative acceleration between k_y and $a(t)$ over each sliding episode. Multiple sliding episodes can occur for a given acceleration-time history, and the cumulative amount of displacement (D) that occurs is a function of multiple characteristics of the time history, including its intensity, frequency content, and duration.

Seismic hazard mapping procedures for landslides integrate topographic, geotechnical, and seismological information to predict sliding displacements, which are then correlated to seismic landslide potential. The procedures currently used for developing seismic landslide hazard maps are limited by the fact that they ignore some of the most critical sources of uncertainties in the analysis. Specifically, the uncertainties in the earthquake ground motion prediction and the sliding displacement prediction are ignored, such that the actual hazard level for seismic landslides is unknown. Recently, Rathje and Saygili (2008, 2009) developed a probabilistic framework for predicting rigid sliding block displacements that incorporates these important uncertainties. Both a scalar approach, which uses one ground motion parameter, and a vector approach, which uses two ground motion parameters, were described. The vector approach reduces the uncertainty in the displacement prediction because of the additional information provided by the second ground motion parameter, making it an attractive alternative.

This paper reviews the probabilistic approaches developed by Rathje and Saygili (2009) and presents their application to seismic landslide hazard mapping. Additionally, current seismic landslide mapping procedures are described and their main shortcomings outlined. The probabilistic approaches are used to develop seismic landslide hazard maps for the Mint Canyon Quadrangle in Southern California, and these maps are compared with those developed using current mapping procedures.

It should be noted that the probabilistic seismic landslide hazard maps derived in this work do not purport to predict the landslide distribution for a specific earthquake event. The

probabilistic approach considers the displacements from all potential regional earthquake magnitude and distance combinations (rather than a single event), which is similar to ground motion hazard maps. In the same way that recorded ground motions from a single earthquake do not validate a ground motion hazard map, observations of earthquake-induced landslides from a single earthquake do not validate probabilistic landslide hazard maps. However, observations of earthquake-induced landslides during previous earthquakes can validate the displacement predictive models used in the probabilistic approach. This issue of validation will be addressed in future work.

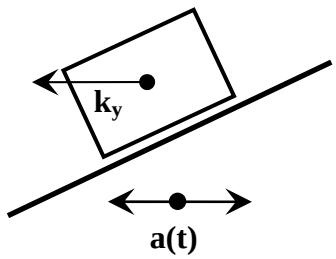

(a)

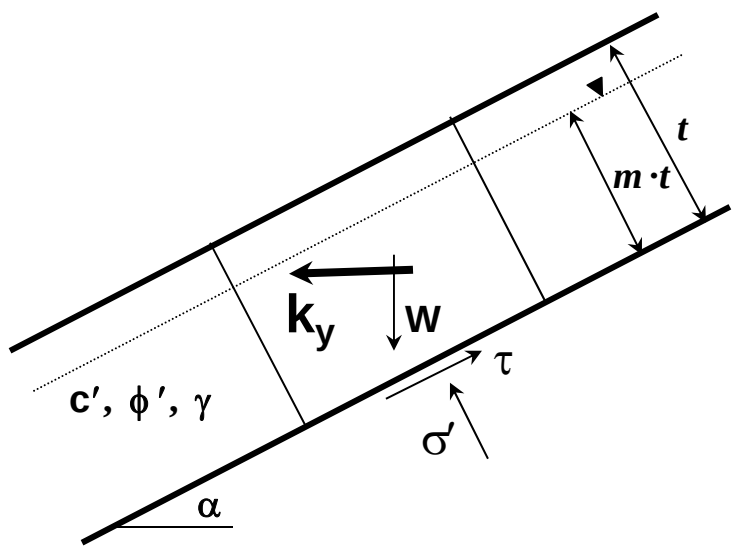

(b)

Figure 1. (a) Rigid sliding block model and (b) infinite slope representation used to define k_y

CURRENT PROCEDURES FOR SEISMIC LANDSLIDE HAZARD MAPPING

Current procedures that are used to develop seismic landslide hazard maps generally use the workflow outlined in Figure 2. The first step is to develop a map of yield acceleration across the study area. Using an infinite slope model (Figure 1b), k_y can be explicitly described as:

$$k_y = \frac{(FS-1)g}{(cos\alpha.tan\phi'+1/tan\alpha)} \tag{1}$$

$$FS = \frac{c'}{\gamma \cdot t \cdot sin\alpha} + \frac{tan\phi'}{tan\alpha} - \frac{\gamma_w \cdot m \cdot tan\phi'}{\gamma \cdot tan\alpha} \tag{2}$$

where k_y is the yield acceleration in the horizontal direction in units of g (g = acceleration of gravity), FS is the static factor of safety, α is the slope angle, ϕ' is the effective internal friction angle of the soil, c' is the effective cohesion of the soil, γ is the unit weight of the soil, t is the failure surface thickness normal to the slope, γ_w is the unit weight of water, and m is the percentage of failure thickness that is saturated (i.e., saturation ratio). Slightly different expressions for k_y have been used that assume the ground acceleration acts parallel to the slope (e.g., Jibson et al. 2000), but the differences in the computed k_y are minor (Saygili 2008).

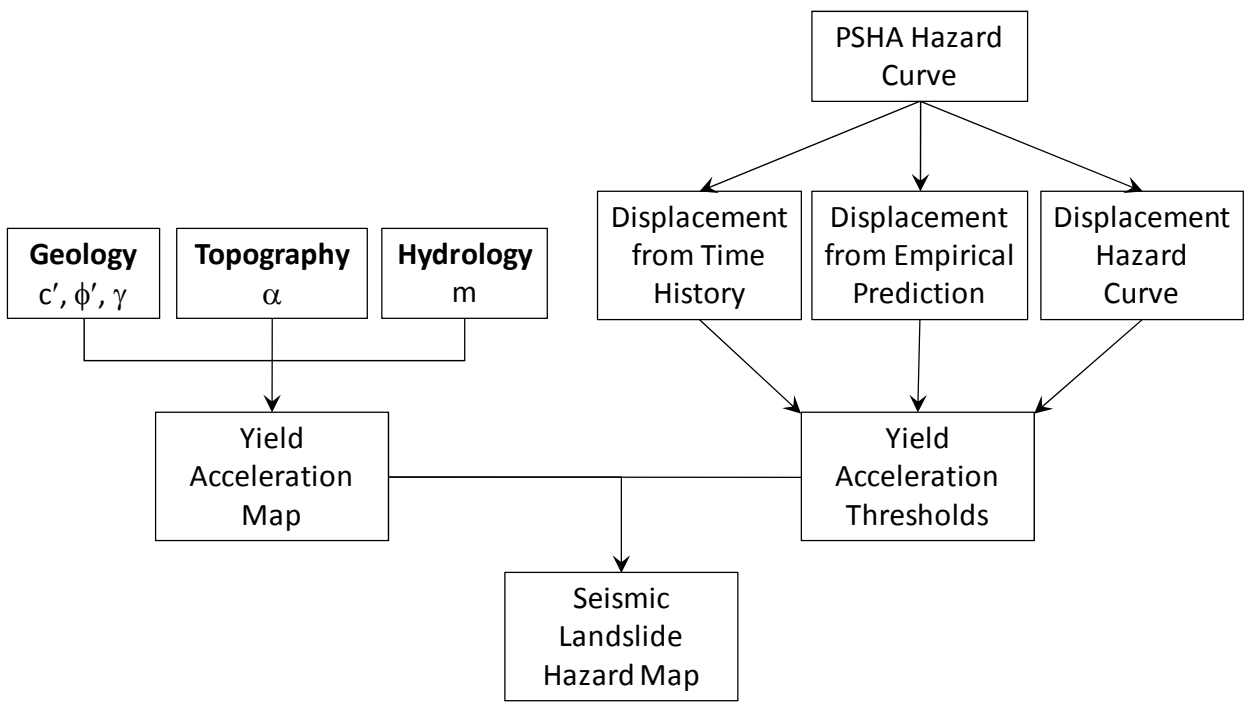

Figure 2. Workflow for developing landslide hazard maps

Each of the parameters used in (1) and (2) must be defined across the study area. A Digital Elevation Model is used to derive slope angles, while geologic maps along with geotechnical data are used to assign shear strength properties (c', ϕ') to the geologic units throughout the region. The unit weight and failure surface thickness typically are assumed, and the saturation ratio (m) can be derived from precipitation information and judgment, or more rigorous

hydrologic analysis (Saygili 2008). Values of k_y, spaced at approximately 10 m intervals, are derived using all of the compiled information. The k_y information essentially is a map of earthquake-induced landslide susceptibility, because it does not take into account the expected level of ground shaking.

The k_y map is combined with earthquake shaking information to develop a map of seismic landslide potential by developing threshold k_y values that are associated with different levels of D for given ground shaking levels. These k_y thresholds generally correspond to the displacement and hazard levels developed by the CGS (Table 1). The k_y thresholds are a function of the expected characteristics of earthquake shaking. For example, if large intensity shaking is expected then slopes with large and small values of k_y will be expected to displace significantly. Alternatively, if small intensity shaking is expected then only slopes with small values of k_y will be expected to displace. Combining the k_y thresholds with the mapped values of k_y allows one to assign each location to a seismic landslide hazard zone based on Table 1. Often seismic landslide hazard maps combine the low, moderate, and high hazard zones into a single landslide hazard zone, such that the D = 5 cm threshold is the most critical for mapping purposes.

Table 1. Landslide hazard criteria used by CGS

Landslide Hazard	**Sliding Displacement (cm)**
Very Low	< 5 cm
Low	5cm < D < 15cm
Moderate	15cm < D < 30cm
High	D > 30cm

The key to developing seismic landslide hazard maps is the approach used to define the k_y thresholds. Currently, two general approaches are used (Figure 2). One approach, which is used by the CGS (McCrink 2001), is based on a single ground motion acceleration-time history. Here, a single acceleration-time history is selected and used to compute D for several values of k_y. The k_y thresholds are defined based on the k_y values that result in the displacement values from Table 1. The selection of the acceleration-time history is guided by the results of a probabilistic seismic hazard analysis (PSHA). Using the peak ground acceleration (PGA) that has a 10% probability of exceedance in 50 years and the modal magnitude and distance combination from the deaggregation of the ground motion hazard, a ground motion acceleration-time history is selected that generally fits these criteria. Using the PSHA-derived ground motion information attempts to incorporate some of the ground motion uncertainty, but using a single acceleration-time history completely ignores the fact that different time-histories can generate significantly different levels of D, even if the motions are selected based on the same seismological criteria. Saygili and Rathje (2008), as well as other (e.g., Jibson 2007, Bray and Travasarou 2007), have shown that for a given value of PGA there is significant variability in the displacement predicted from different time histories. Therefore, developing k_y thresholds from a single acceleration-time history should be avoided.

A second approach to developing k_y thresholds is to use an empirical model that predicts D as a function of k_y and one or more ground motion parameters (e.g., PGA, Arias Intensity I_a, peak ground velocity PGV). There are many available predictive models, but the most recently developed models are Rathje and Saygili (2009), Saygili and Rathje (2008), Jibson (2007), and Bray and Travasarou (2007). To account for ground motion uncertainty, the ground motion level

used in the predictive model is derived from the PSHA and is often taken as either the 10% in 50 year or the 2% in 50 year value. Because the ground motion level is based on PSHA, this approach is considered pseudo-probabilistic (Rathje and Saygili 2008). The median displacement prediction from the empirical model is used to identify the k_y thresholds from the ground motion level. Using an empirical predictive model is an improvement over using a single time history because the median displacement is more stable than a value derived from a single time history. However, each of these predictive models has a large standard deviation such that the range of expected displacements for a given k_y and ground motion level is often greater than one order of magnitude. This source of uncertainty in generally neglected in this approach.

In addition the approaches above, Jibson et al. (2000) considered the probability that a failure occurs given the predicted level of displacement. The relationship between probability of failure and displacement level was derived from the observed landslides from the Northridge earthquake and the median displacement predicted from an empirical predictive model and contours of ground motion levels from ground motion recordings in the area. Even for the largest displacements calculated by the empirical model, the landslide inventory indicated only a 35% probability of failure. While this small probability of failure for a large level of displacement may lead one to initially question the methodology of predicting earthquake-induced landslide hazards, it should be noted that an area covered with 35% landslides is massively destroyed. This small value of probability is a result of natural spatial variability in shear strength within a geologic unit, as well as uncertainty in the ground motion intensity across the study area, and some of this variability may never be reduced when considering landslides on a regional scale.

PROBABILISTIC APPROACH FOR SEISMIC LANDSLIDE HAZARD MAPPING

The pseudo-probabilistic approach discussed above uses the PSHA seismic hazard curve to derive a single ground motion value for use in an empirical predictive model. A fully probabilistic approach convolves the full ground motion hazard curve with the displacement predictive model and its variability to develop a hazard curve for D for a given value of k_y. The hazard curve is a plot of the mean annual rate of exceedance (λ_D) for different levels of D. Then, the displacement level with a specific hazard level (i.e., 10% probability of exceedance in 50 years, λ = 0.0021 1/yr) can be used to assign the seismic landslide hazard potential. The pseudo-probabilistic approach essentially uses a ground motion with a specific hazard level and assumes the median displacement is associated with the same hazard level. Rathje and Saygili (2008) showed that this assumption is generally incorrect and nonconservative.

Scalar probabilistic approach

If the predictive model for D is represented as a function of a single ground motion parameter (GM), a scalar probabilistic approach is used. For this case, the mean annual rate of exceedance (λ_D) for a displacement level x is defined as:

$$\lambda_D(x) = \sum_i P[D > x|GM_i] \cdot P[GM_i] \tag{3}$$

where $P[D > x|GM_i]$ represents the probability that displacement level x is exceeded when the ground motion level is equal to GM_i. This value is derived from the displacement predictive model and its standard deviation. $P[GM_i]$ is the annual probability of occurrence of ground

motion level GM_i. Note that annual rates of exceedance/occurrence (λ) and annual probabilities (*P*) are used interchangeably because for rare events these values are essentially equal. The summation in (3) is performed over bins that span the full range of ground motion levels. Various empirical predictive models could be used with (3) to develop a displacement hazard curve, including Saygili and Rathje (2009), Jibson (2007), and Bray and Travasarou (2007).

Equation (3) requires the discrete annual probabilities of occurrence, not exceedance, of different ground motions levels. This information represents a probability mass function and can be derived from the output from a PSHA code using:

$$P[GM_i] = \frac{\lambda_{GM,i}+\lambda_{GM,i-1}}{2} - \frac{\lambda_{GM,i}+\lambda_{GM,i+1}}{2} = \frac{\lambda_{GM,i-1}-\lambda_{GM,i+1}}{2} \tag{4}$$

where $\lambda_{GM,i-1}$, $\lambda_{GM,i}$, and $\lambda_{GM,i+1}$ represent adjacent hazard values for ground motion (λ_{GM}) centered about ground motion level GM_i. Figure 3(a) displays a hazard curve for PGA for a site in Southern California. The associated discrete values of annual probability of occurrence for PGA based on the hazard curve are shown in Figure 3(b), and shows that the probability of occurrence decreases as PGA increases. Note that the discrete probabilities are a function of the size of the ground motion bins (i.e., the difference between successive PGA values in a hazard curve).

Equation (3) assumes that the displacement predictive model is sufficient (Cornell and Luco 2001); i.e., the model sufficiently predicts displacement in terms of *GM* without the need for specifying the earthquake magnitude or site-to-source distance. Rathje and Saygili (2009) showed that when using only PGA to predict *D*, the predictive model must also include earthquake magnitude as a predictor variable if the prediction is to be unbiased. For this case, (3) is modified to account for magnitude (Rathje and Saygili 2009, Luco 2002):

$$\lambda_D(x) = \sum_i \sum_j P[D > x | GM_i, M_j] \cdot P[M_j | GM_i] \cdot P[GM_i] \tag{5}$$

where $P[D > x | GM_i, M_j]$ represents the probability of $D > x$ given ground motion level GM_i and earthquake magnitude M_j, and $P[M_j | GM_i]$ is the probability of occurrence of M_j given ground motion level GM_i. $P[M_j | GM_i]$ can be derived from the hazard deaggregation for GM_i. The magnitude deaggregation for the site in Southern California is shown in Figure 3(c) for the λ_{GM} = 0.0021 1/yr ground motion. In this case, the hazard is dominated by events between M = 6.6 and 7.4. The summations in (5) are performed over bins that span all ground motion levels and magnitudes. Rathje and Saygili (2009) presented a displacement predictive model as a function of PGA and M that can be used with (5) to develop a displacement hazard curve.

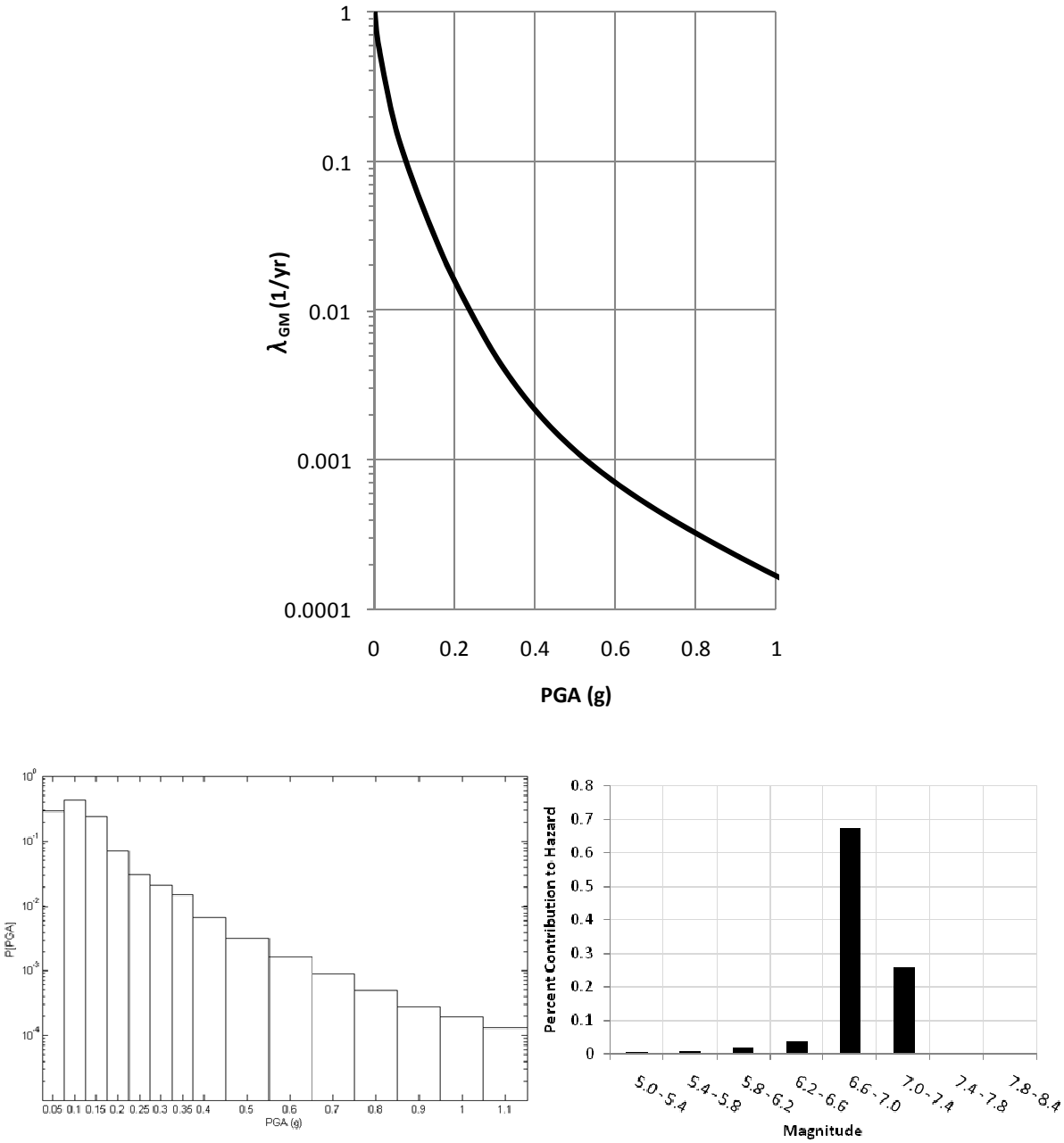

Figure 3. (a) PGA hazard curve, (b) Annual Probabilities of Occurrence, and (c) Magnitude deaggregation at λ_{GM}=0.0021 1/yr for a site in Southern California.

Vector probabilistic approach

If the predictive model for *D* is represented as a function of two ground motion parameters (*GM1* and *GM2*), a vector probabilistic approach is used. For this case, the mean annual rate of exceedance for a displacement level *x* is defined as:

$$\lambda_D(x) = \sum_i \sum_k P[D > x | GM1_i, GM2_k] \cdot P[GM1_i, GM2_k] \tag{6}$$

where $P[D > x | GM1_i, GM2_k]$ represents the probability of $D > x$ given ground motion levels $GM1_i$ and $GM2_k$, and $P[GM1_i, GM2_k]$ is the joint annual probability of occurrence of ground motion levels $GM1_i$ and $GM2_k$. The double summation is performed over bins for both ground motion parameters. Saygili and Rathje (2008) developed a suite of empirical models that use different pairs of ground motion parameters to predict displacement and can be used in (6). The model recommended by Saygili and Rathje (2008) uses PGA and PGV, and has a significantly smaller standard deviation than the model that uses PGA and M.

The joint annual probabilities of occurrence are computed via a vector PSHA (VPSHA) for the ground motion hazard (e.g., Bazzuro and Cornell 2002). Alternatively, the VPSHA can be approximated from the scalar PSHA for one of the ground motion parameters, the hazard deaggregation for that ground motion parameter, and ground motion prediction equations for *GM1* and *GM2* (Bazzurro 1998, Rathje and Saygili 2009). For either approach, the VPSHA requires an estimate of the correlation coefficient between *GM1* and *GM2*.

Figure 4 displays the VPSHA joint annual probabilities for PGA and PGV computed for a site in Southern California. The correlation coefficient between PGA and PGV was taken as 0.6, based on Rathje and Saygili (2008). The VPSHA results indicate that pairs of smaller values of (PGA, PGV) have larger probabilities of occurrence, while pairs of larger values of (PGA, PGV) have smaller probabilities. This result is similar to the scalar PSHA results (Figure 3(b)). Additionally, the probability of a small value of PGA occurring with a large value of PGV (and vice versa) is very small.

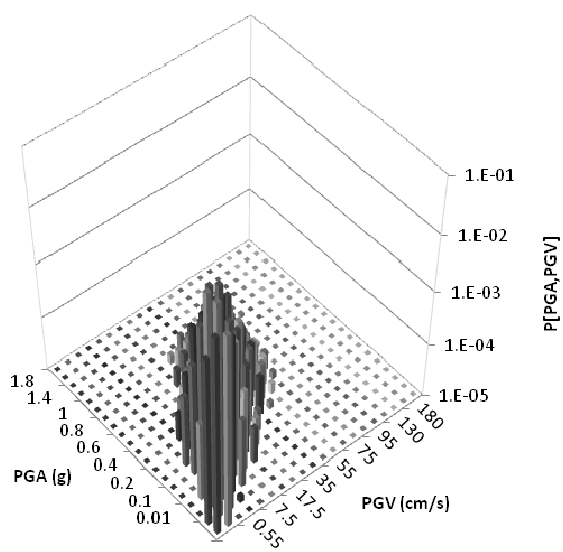

Figure 4. Joint annual probabilities of occurrence for PGA, PGV pairs for a site in Southern California

Displacement Hazard Curves

Figure 5 displays displacement hazard curves for k_y = 0.15 g using the ground motion hazard information from Figures 3 and 4. The scalar model that incorporates PGA and M (Rathje and Saygili 2009) was used to develop one curve, while the vector model that incorporates PGA and PGV (Saygili and Rathje 2008) was used to develop the other. The vector (PGA, PGV) hazard curve results in significantly smaller displacement levels than the scalar (PGA, M) curve. At λ_D = 0.0021 1/yr (10% probability of exceedance in 50 years), the scalar model predicts 90 cm of displacement while the vector model predicts 20 cm. At λ_D = 0.0004 1/yr (2% probability of exceedance in 50 years), the scalar model predicts 280 cm of displacement while the vector model predicts 60 cm. Generally, the displacement hazard is reduced by more than a factor of four when the vector model is used (Rathje and Saygili 2008, 2009). The smaller displacement values for the vector model are caused by the vector model predicting smaller median displacements than the scalar model, as well as the vector model having a smaller standard deviation.

For seismic landslide hazard mapping, yield acceleration thresholds that are associated with different displacement thresholds are required (Figure 2). When implementing the probabilistic approaches to define k_y thresholds, displacement hazard curves are generated for a suite of k_y values such that the k_y values that predict the displacement thresholds at a specified hazard level (λ_D) can be identified. The most common hazard levels considered are 0.0021 1/yr (10% in 50 years) and 0.0004 1/yr (2% in 50 years).

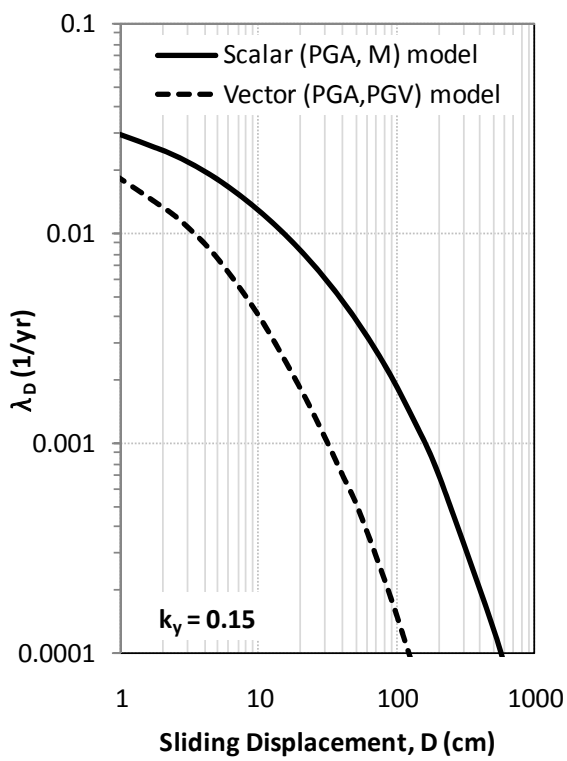

Figure 5. Displacement hazard curves derived from scalar and vector probabilistic approaches for k_y = 0.15 g. Ground motion hazard from Figures 3 and 4.

APPLICATION OF PROBABILISTIC APPROACHES TO A QUADRANGLE IN CALIFORNIA

Study Area

To demonstrate the probabilistic approaches, a quadrangle in California was selected for study. In consultation with the CGS, the Mint Canyon 7.5 minute quadrangle in Southern California was chosen. This quadrangle is located in Los Angeles County in Southern California (Figure 6), and it is centered at 34.437° N, 118.438° W (CDMG 1998). Within the quadrangle, the minimum and maximum elevations above mean sea level are 386 m and 1,044 m. This quadrangle was selected based predominantly on the availability of a significant amount of shear strength data, and the fact that the CGS landslide hazard map for that quadrangle had been updated relatively recently (2001).

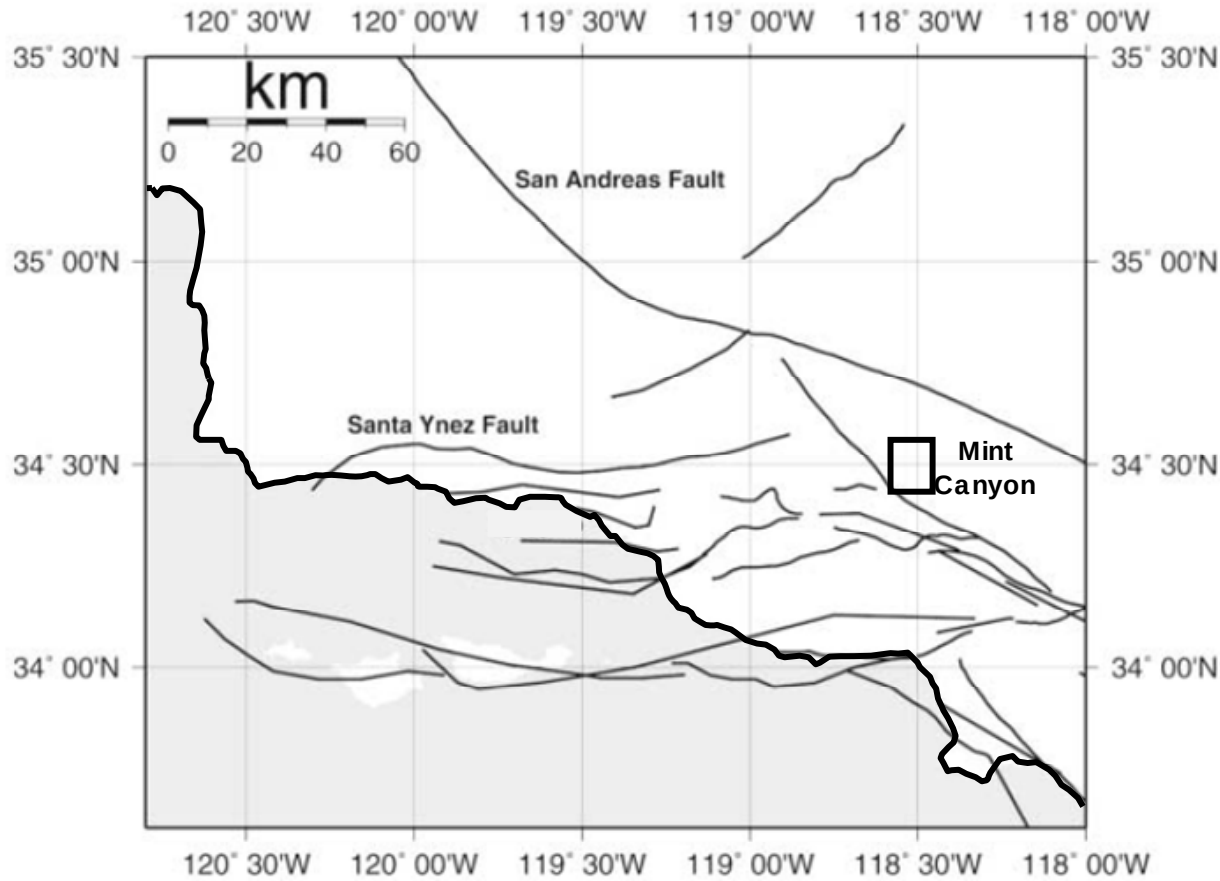

Figure 6. Locations of Mint Canyon Quadrangle and faults in Southern California (modified from Bazzurro and Cornell 2004).

Topographic and shear strength information for the quadrangle were supplied by the CGS (Figure 7). The Santa Clara River flows to the west across the center of the quadrangle and much of the quadrangle is mountainous terrain cut by numerous canyons. The southeast corner of the quadrangle and the northern boundaries have areas of steep relief (CDMG 1998). The slope angles are shown in Figure 7(a). The distribution of slope angles within the quadrangle

indicates that about 55% of the slopes are less than 15°, 26.5% are between 15° and 25°, 15% are between 25° and 35°, and 3.5% are steeper than 35°. The steepest slope in the quadrangle is about 68°.

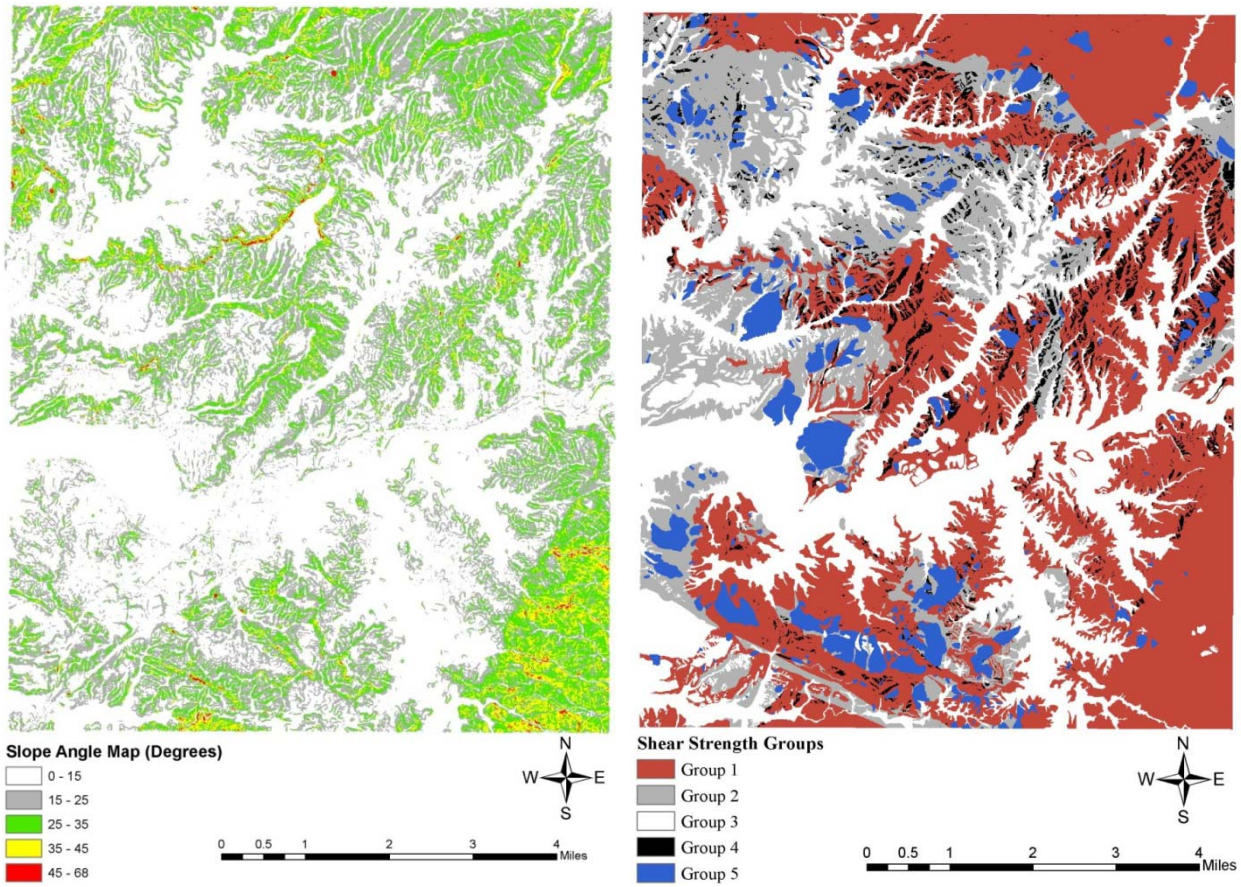

Figure 7. Slope angles and shear strength groups for the Mint Canyon Quadrangle.

CGS compiled and digitized geologic maps from various resources and processed these maps to reflect the most recent geologic mapping in the area. The geologic units in the quadrangle include Pre-Cambrian and Pre-Cenozoic igneous units, Tertiary to Pleistocene sedimentary units, and Quaternary soil deposits (CDMG 1998). The geologic units are listed in Table 2. CGS grouped the geologic units into five shear strength groups based on their shear strength and lithologic character (Table 3). For geologic units with adequate data (results from over 400 tests were available for this quadrangle), average internal friction angles (ϕ') were compared for grouping. If the average values of ϕ' between two groups were within two degrees, these units were combined into the same strength group. For geologic units with little or no shear test data, only lithologic similarities were considered for grouping. Additionally, the effect of adverse bedding conditions (i.e., locations where bedding dips at approximately the same angle and direction of the slope) was considered for the sedimentary units. Locations with adverse bedding conditions were assigned smaller shear strength parameters than for the rest of that geologic unit. The final geologic strength groups (Table 3) generally represent Tertiary (and older) deposits with favorable bedding (Group 1), weaker Tertiary deposits coupled with stronger Quaternary

deposits (Group 2), Quaternary deposits (Group 3), Tertiary units with adverse bedding conditions (Group 4), and existing landslides (Group 5). The geographic distribution of the five strength groups is shown in Figure 7(b).

Table 2 Geologic units in the Mint Canyon Quadrangle

Geologic Unit	Symbol
Gabbro	gb
Gneiss	gn
Granite	gr
Pelona schist	ps
Placerita Formation	pm
Granodiorite	gd
Vasquez Formation	Tvz Tvv
Tick Canyon Formation	Ttk
Mint Canyon formation	Tmc1 Tmc2 Tmc3 T
Castaic Formation	Tcs
Towsley Formation	Tw Twc
Saugus Formation (Sunshine Ranch Member)	Tsru Tsrl
Saugus Formation	Qs Qsc Qsg
Pacoima Formation	Qpa
Terrace deposits	Qt
Older colluvium	Qco
Fan deposits	Qf
Floodplain deposits	Qfp
Alluvium	Qal
Colluvium	Qc
Slope wash deposits	Qsw
Pond deposits	Qp
Modern man-made fill	af
Artificial cut and fill	afc

Table 3 Geologic strength groups for the Mint Canyon Quadrangle

Group 1	Group 2	Group 3	Group 4	Group 5
gr, gb, gd ps, pm, gd Tvz (fbc), Tvv (fbc) T (fbc) Tmc1 (fbc) Tmc3 (fbc) Tcs (fbc) Tw (fbc), Twc (fbc) Tsrl (fbc) Tsru (fbc) Qsg (fbc), Qsc (fbc)	Ttk (fbc) Tmc2 (fbc) Qs (fbc)	Qs (abc) Qsg (abc), Qsc (abc) Qpa, Qt Qco, Qf, Qfp Qsw, Qc, Qal af, afc	Tvz (abc), Tvv (abc) T (fbc), Ttk (abc) Tmc1 (abc) Tmc2 (abc) Tmc3 (abc) Tcs (abc) Tw (abc) Tsrl (abc) Tsru (abc) Qp	Qls

The results from over 400 shear strength tests (mostly direct shear) were provided by CGS, and were used to independently evaluate the shear strength parameters (c′, ϕ′) for the shear strength groups. 222 out of the 400 shear strength tests were performed on samples from shallow depth (less than 3 m) and these were selected for study because they are representative of shallow, infinite slope conditions. Table 4 lists the shear strength parameters derived from the laboratory data for the five shear strength groups. In terms of ϕ′, Group 1 is the strongest (34°) and Group 5 the weakest (16°). The c′ values vary from about 10 kPa to 20 kPa. Jibson et al. (2000) developed seismic landslide maps in quadrangles immediately west of Mint Canyon (e.g., Oat Mountain, Newhall) and these quadrangles contain many of the same geologic units as Mint Canyon. The shear strength parameters derived by Jibson et al. (2000) for the tertiary units listed in Table 2 are similar to those used in this study (Group 1, fbc). For the other geologic units common to the studies, the shear strength parameters used here are consistently smaller than Jibson et al. (2000). These differences can be ascribed to the availability of different shear strength datasets, different interpretations of shear strength data, and different geologic strength groups.

There are some issues regarding the use of the cohesion intercept in evaluating k_y. The CGS ignores cohesion in developing their k_y maps because they found in their validation studies that the best comparison with observed earthquake-induced landslides was obtained with c′ = 0 kPa (McCrink 2001). Additionally, the cohesion intercept from poor quality laboratory tests (i.e., not fully saturated, not fully drained) may not be representative of field conditions, and thus using these values of c′ will result in unrealistic values of k_y. However, when c′ is completely ignored, it is common to have many areas with $k_y < 0.0$. This condition indicates that the slopes are statically unstable, which is not realistic for areas that have not failed. Therefore, a rational assessment of c′ is needed.

For this study, the shear strength and slope angle information across the quadrangle was used to develop an initial map of yield acceleration using (1) and (2). The other parameters in (1) and (2) were taken as $\gamma = 15.7$ kN/m^3, t = 2.4 m (shallow failures, Jibson et. al. 2000), and $m = 0$ (dry conditions). When ignoring c′, approximately 11% of the quadrangle displayed $k_y < 0.0$. Other

quadrangles studied showed up to 30% of the quadrangle as statically unstable (Saygili 2008). When the laboratory measured values of c′ were included for the Mint canyon quadrangle, almost all of the slopes became statically stable and all of the k_y values increased. In fact, almost no slopes displayed $k_y < 0.3$ when the laboratory c′ values were included, indicating that little of the quadrangle was susceptible to seismic failure. Because of the uncertainty in the accuracy of the laboratory measured values of c′, an additional set of c′ values were back-calculated by constraining FS=1.0 for the larger slope angles in each geologic strength group (Saygili 2008). The constrained values of c′ are listed in Table 4, and are about one-half of the laboratory values.

Table 4 Summary of the shear strength parameters for the geologic strength groups in the Mint Canyon Quadrangle

Group	No. of Tests	Laboratory Data		Constrained
		ϕ′ (°)	c′ (kPa)	c′ (kPa)
Group 1	43	34°	15.4	8.8
Group 2	23	30°	14.3	9.9
Group 3	94	28°	13.6	7.5
Group 4	58	22°	21.1	9.3
Group 5	4	16°	11.9	11.6

Development of Yield Acceleration Thresholds

The scalar and vector probabilistic methods were used to develop yield acceleration thresholds associated with D = 5 cm, 15 cm, and 30 cm. The PSHA hazard curves for PGA and the VPSHA data for PGA and PGV were computed at nine locations within the quadrangle, each separated by approximately 0.05°. The PSHA and VPSHA codes from Dr. Norman Abrahamson (personal communication) were used for these calculations. The seismicity of the region was characterized by a group of active sources, including 18 faults within 180 km of the site (N. Gregor, personal communication). The ground motion prediction equations of Boore and Atkinson (2008) were used, and soft rock conditions were assumed (V_{s30}=760 m/s). The nine hazard curves across the quadrangle for PGA are shown in Figure 8. The hazard curves for locations 1 through 6 are similar, with the hazard curves for locations 7 through 9 slightly larger. The larger hazard at these locations is due to their proximity to the faults south of the quadrangle (Figure 6). Generally, the seismic hazard at this site is high, with the 475 year return period (λ = 0.0021 1/yr) PGA around 0.4 to 0.5 g, the 975 year return period (λ = 0.001 1/yr) PGA around 0.5 to 0.6 g, and the 2475 year return period (λ = 0.0004 1/yr) PGA around 0.6 to 0.8 g.

The displacement hazard curves derived from the PSHA and VPSHA ground motion information at location 1 are shown in Figure 9 for multiple values of k_y. Considering a hazard level of 10% probability of exceedance in 50 years (λ_D = 0.0021 1/yr), k_y thresholds of 0.21 g, 0.16 g, and 0.12 g correspond to displacement thresholds of 5, 15, and 30 cm, respectively, when using the scalar PSHA approach (Figure 9(a)). For the same hazard level (λ_D = 0.0021 1/yr) using VPSHA, yield acceleration thresholds of 0.13 g, 0.08 g, and 0.06 g correspond to the same displacement thresholds (Figure 9(b)). The VPSHA k_y thresholds are smaller than the PSHA thresholds, such that application of the VPSHA thresholds will result in smaller landslide hazard zones.

Using these k_y thresholds, gridded values of k_y across the quadrangle are placed in the appropriate displacement and landslide potential bins (Table 5). When considering all nine ground motion locations across the quadrangle, k_y thresholds are defined for each ground motion location and the gridded k_y values are compared with the k_y thresholds from the closest ground motion location. For the other ground motion locations within the quadrangle that displayed slightly larger hazard (e.g., locations 7-9), the k_y thresholds were about 0.02 g to 0.03 g larger than those shown in Table 5.

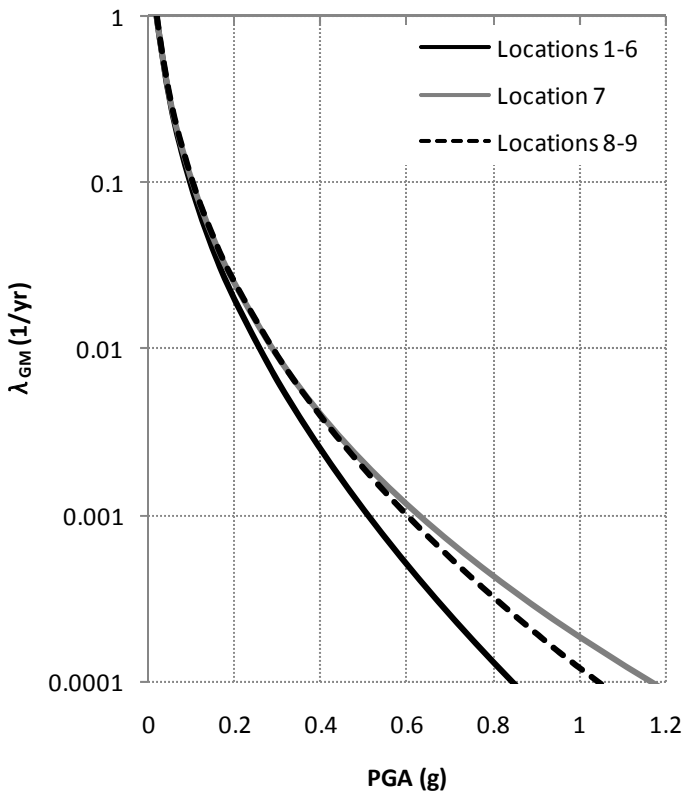

Figure 8. PGA hazard curves for the nine locations within the quadrangle

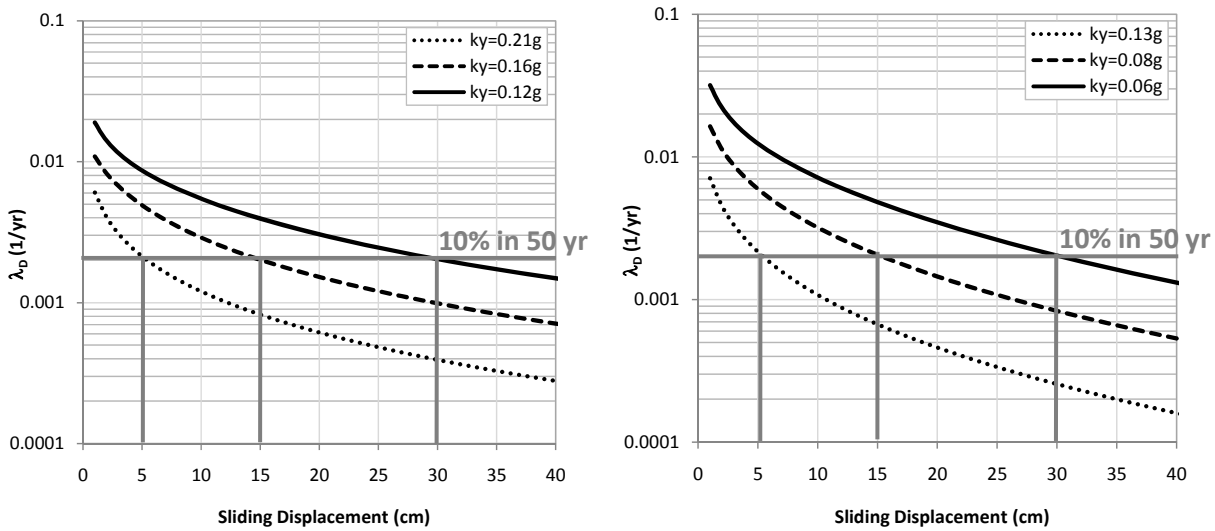

Figure 9: Displacement hazard curves for varying yield acceleration values for (a) PSHA, and (b) VPSHA

Table 5 The yield acceleration thresholds for scalar and vector approaches at λ_D = 0.0021 1/yr

D	***Landslide Hazard***	***k_y Thresholds (Scalar PSHA)***	***k_y Thresholds (Vector PSHA)***
< 5 cm	Very Low	> 0.21 g	> 0.13 g
5-15 cm	Low	0.16-0.21 g	0.08 -0.13 g
15-30 cm	Medium	0.12-0.16 g	0.06-0.08 g
>30 cm	High	< 0.12 g	< 0.06 g

Seismic Landslide Hazard Maps

Seismic landslide hazard maps were developed for the Mint Canyon quadrangle using probabilistic and pseudo-probabilistic approaches. These maps are discussed and described below. All of the maps represent a hazard level of 10% probability of exceedance in 50 years (λ = 0.0021 1/yr).

The scalar and vector k_y thresholds (Table 5) were used with the constrained shear strength parameters (Table 4) to assign locations to displacement bins representing < 1 cm, 1-5 cm, 5-15 cm, 15-30 cm, and > 30 cm. Figures 10 (a) and (b) display the geographic distribution of *D* values across the quadrangle from these analyses. These figures indicate that the most significant hazard (with the largest displacements) is associated with the steeper slopes in the northern and southeast sections of the quadrangle (> 25°, Figure 7). The area of landslide hazard is smaller when using the vector approach (Figure 10b) than when using the scalar approach (Figure 10a). This observation is quantitatively demonstrated in Table 6, which lists the percentages of the quadrangle assigned to different displacement bins from the scalar and vector approaches, as well as the total area associated with *D* > 5 cm. These data indicate that when using the vector approach, the area with *D* > 5 cm is reduced by about 50% (5.4% vector vs. 11.1% scalar). This reduction is associated with an increase in the area encompassed in the *D* < 5 cm displacement bin.

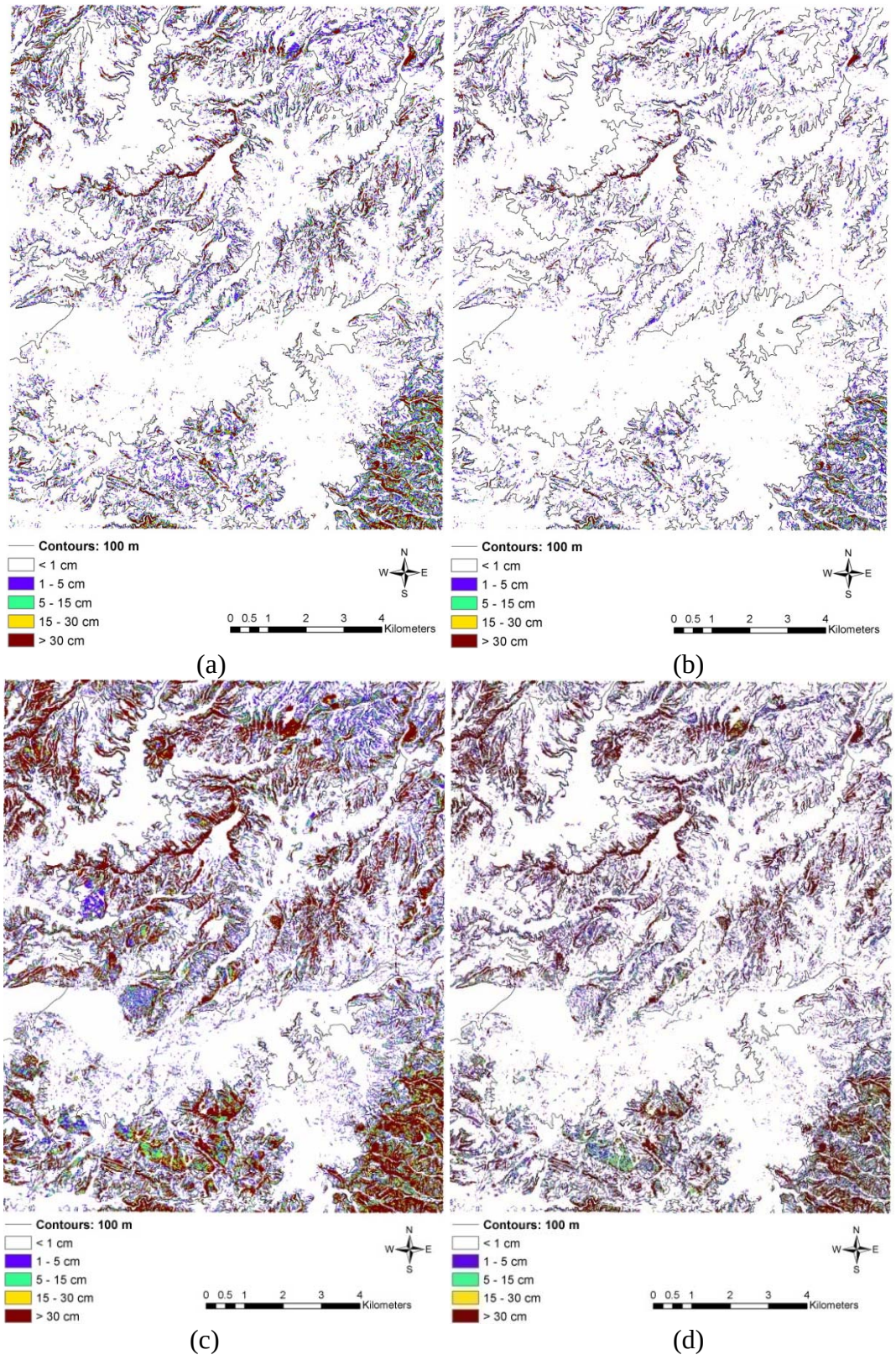

Figure 10. Displacement levels derived from (a) scalar approach with c′=contrained, (b) vector approach with c′= contrained, (c) scalar approach with c′=0, (d) vector approach with c′=0.

Table 6 Percentage of the quadrangle assigned to different displacement bins for scalar and vector approaches (λ_D = 0.0021 1/yr).

	Landslide Displacement Bins	*Percentage of the quadrangle* Strength Case c′ = constrained	Strength Case c′ = 0
Scalar Approach	< 5 cm	88.9%	59.2%
	5 - 15 cm	5.0%	9.5%
	15 - 30 cm	2.0%	5.5%
	> 30 cm	4.1%	25.8%
	Total > 5 cm	***11.1%***	***40.8%***
Vector Approach	< 5 cm	94.6%	70.8%
	5 - 15 cm	2.6%	7.7%
	15 - 30 cm	1.0%	4.0%
	> 30 cm	1.8%	17.5%
	Total > 5 cm	***5.4%***	***29.2%***
Empirical Model	< 5 cm	92.0%	--
	5 - 15 cm	3.8%	--
	15 - 30 cm	1.6%	--
	> 30 cm	2.6%	--
	Total > 5 cm	***8.0%***	**--**

As discussed earlier, the CGS assigns c′ = 0 to all geologic units when developing seismic landslide hazard maps. For this quadrangle, this assumption results in 11% of the quadrangle being statically unstable (k_y < 0.0). To demonstrate the significant effect that the assumed c′ values has on the landslide hazard map, a set of maps was derived using c′=0. Gridded k_y values were computed using the ϕ′ values in Table 4 coupled with c′ = 0, and these k_y values were compared with the k_y thresholds from the scalar and vector probabilistic approaches (Figures 10 (c) and (d)). The distribution of the displacement bins are listed in Table 6. Ignoring c′ significantly increases the landslide hazard in both the scalar and vector approaches, such that each of the displacement bins associated with landslide hazard (5-15 cm, 15-30 cm, and > 30 cm) increases and the area with D > 5 cm increases by factors of 3.5 to 5.5 (Table 6). The increase is larger for the vector approach. The increase is most significant for the D > 30 cm bin, mostly because this is influenced by the k_y < 0.0 areas. Thus, it is clear that the selection of c′ is critical in developing seismic landslide hazard maps.

Finally, a map of D values was generated using the median displacement from an empirical prediction model. In this case, the 10% in 50 year PGA and associated earthquake magnitude (M) from PSHA deaggregation was used with the empirical predictive model of Rathje and Saygili (2009). This approach is the same as the approach used by Jibson et al.

(2000), except that a different empirical predictive model is used. The geographic distribution of *D* values using this approach are displayed in Figure 11 and listed in Table 6. The percentage of the quadrangle with $D > 5$ cm is 8.0% from the empirical model, as compared with 11.1% for the scalar approach and 5.4% for the vector approach. Therefore, the seismic landslide hazard from the empirical model is smaller than from the scalar approach and larger than from the vector approach. These differences are a consequence of the uncertainty in the displacement prediction. Using the median displacement from the empirical predictive model ignores the uncertainty in the displacement prediction, while the scalar approach incorporates this uncertainty. Incorporating this uncertainty causes the larger hazard zone for the scalar probabilistic approach. The vector approach also incorporates the uncertainty in the displacement prediction, but because this uncertainty is smaller due to the use of multiple ground motion parameters and because the median displacement prediction from the vector model is smaller than from the scalar model (Rathje and Saygili 2009), the seismic landslide hazard zone is smaller for the vector probabilistic approach.

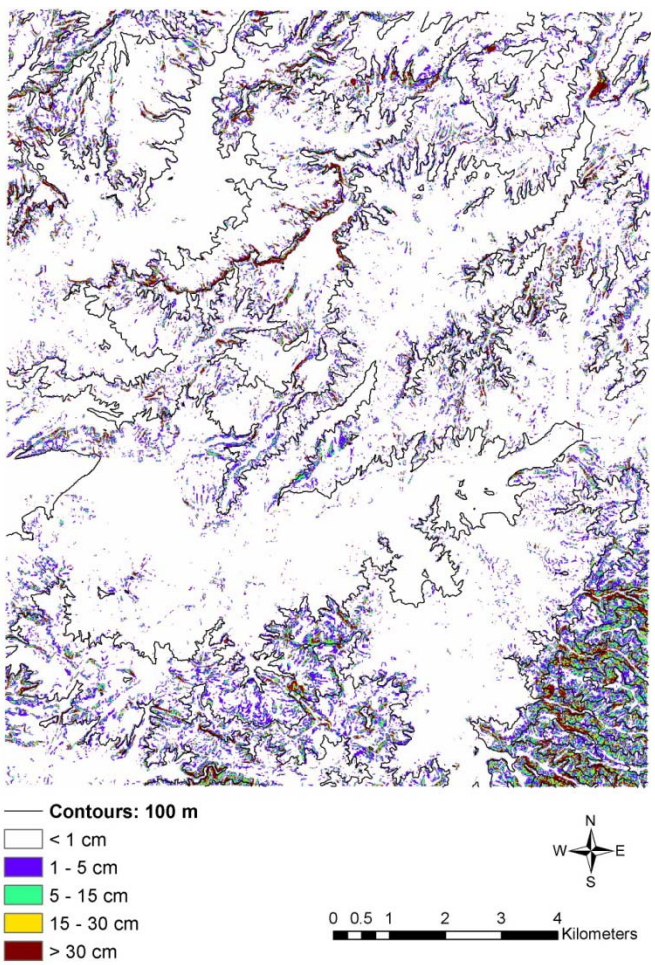

Figure 11. Displacement levels derived from the Rathje and Saygili (2009) empirical model and $\lambda = 0.0021$ 1/ yr PGA and M. Contrained c′ shear strength parameters used.

CONCLUSIONS

Seismic landslide hazard maps are useful tools that guide development and zoning decisions, and provide the motivation for detailed studies of earthquake-induced landslides. Additionally, the Seismic Hazards Mapping Act of California requires that the CGS develop seismic landslide hazard maps. Therefore, it is critical that the procedures used to develop these maps be robust and accurate.

The current procedures used to develop seismic landslide hazard maps suffer from one main limitation: they ignore the uncertainty in the prediction of sliding displacement. While the uncertainties in ground motion prediction are taken into account via PSHA, the displacement prediction is not treated with the same rigor. The probabilistic approaches presented by Rathje and Saygili (2008, 2009) address this shortcoming. Two probabilistic approaches were presented in this work. The scalar probabilistic approach uses PGA and M to predict sliding displacement, while the vector probabilistic approach uses PGA and PGV to predict sliding displacement. The scalar approach can be implemented using the results from traditional PSHA, while the vector approach requires vector PSHA analysis or an estimate of the VPSHA distribution.

The scalar and vector probabilistic analyses produce a displacement hazard curve for a given k_y. Generally, the vector approach results in a smaller displacement hazard for a given k_y than the scalar approach because the vector displacement model has a smaller standard deviation and smaller median displacement prediction. The displacement hazard curves allow one to determine the displacement level associated with a hazard level (i.e. λ_D). When applied to seismic landslide hazard mapping, displacement hazard curves are generated for a range of k_y values such that the k_y values associated with different displacement thresholds at a given λ_D can be assessed.

The probabilistic approaches were used to develop seismic landslide hazard maps for the Mint Canyon quadrangle in Southern California. These maps were compared with maps developed using procedures in common use. For this quadrangle, the scalar approach produced a seismic landslide zone (defined as $D > 5$ cm) about twice as large as the scalar approach. The approach using an empirical predictive model produced a smaller landslide hazard zone than the scalar approach, but a larger zone than the vector approach. It was also demonstrated that the selection of the shear strength parameters considerably affects the resulting seismic landslide hazard map, and thus these values should be selected carefully.

The probabilistic approaches presented and demonstrated here represent rational methods to evaluate earthquake-induced landslide hazards. These methods incorporate the important uncertainties related to ground motion prediction and sliding displacement prediction, and are easily implemented on a regional scale for hazard mapping.

REFERENCES

Bazzurro, P., and Cornell, C. A. (2002). "Vector-valued probabilistic seismic hazard analysis (VPSHA)." *Proc., 7th U.S. National Conf. on Earthquake Engineering*, Vol. II, EERI, Oakland, Calif., 1313–1322.

Bazzurro, P. and Cornell, C.A. (2004) "Nonlinear Soil Site Effects in Probabilistic Seismic Hazard Analysis," *Bulletin of the Seismological Society of America*, 94(6), 2110-2123.

Bazzurro, P., (1998). Probabilistic Seismic Demand Analysis, Ph.D. thesis, Dept. of Civil and Environmental Engineering, Stanford University, California (also available at: http://pitch.stanford.edu/rmsweb/Thesis/PaoloBazzurro.pdf)

Bray, J.D. and Travasarou, T. 2007. "Simplified Procedure for Estimating Earthquake-Induced Deviatoric Slope Displacements," *Journal of Geotechnical and Geoenvironmental Engineering*, ASCE, 133(4), 381-392.

Boore, D. M. and Atkinson, G. M. (2008) "Ground-motion Prediction Equations for the Average Horizontal Component of PGA, PGV and 5%-Damped PSA at Spectral Periods between 0.01 s and 10.0 s," *Earthquake Spectra*, EERI, 24(1), 99-138.

California Division of Mines and Geology, CDMG (1998) "Seismic hazard zone report for the Mint Canyon 7.5-Minute Quadrangle, Los Angeles County, California," available at http://gmw.consrv.ca.gov/shmp/download/evalrpt/mintc_eval.pdf

Cornell, C. A., and Luco, N., (2001) "Ground motion intensity measures for structural performance assessment at near-fault sites," Proceedings of the U.S.-Japan joint workshop and third grantees meeting, U.S.-Japan Coop. Res. on Urban EQ. Disaster Mitigation, Seattle, Washington.

Jibson, R.W., Harp, E.L., and Michael, J.A. (2000), "A Method for Producing Digital Probabilistic Seismic Landslide Hazard Maps," *Engineering Geology* **58**, 271–289.

Jibson, R.W., (2007) "Regression models for estimating coseismic landslide displacement." *Engineering Geology*, 91, 209–218.

Luco N. (2002) "Probabilistic Seismic Demand Analysis, SMRF Connection Fractures, and Near-source Effects" Ph.D. Dissertation, Department of Civil and Environmental Engineering, Stanford University, CA.

McCrink, T.P., (2001) "Mapping earthquake-induced landslide hazards in Santa Cruz County" in Ferriz, H. and Anderson, R., editors, *Engineering geology practice in northern California: California Geological Survey Bulletin 210 / Association of Engineering Geologists Special Publication 12*, p.77-94.

Rathje, E.M. and Saygili,G. (2008) "Probabilistic Seismic Hazard Analysis for the Sliding Displacement of Slopes: Scalar and Vector Approaches," *Journal of Geotechnical and Geoenvironmental Engineering*, ASCE, 134(6), 804-814.

Rathje, E.M., and Saygili, G. 2009. "Probabilistic Assessment of Earthquake-Induced Sliding Displacements of Natural Slopes," *Bulletin of the New Zealand Society of Earthquake Engineering*, 41, 18-27.

Saygili, G. (2008) "A Probabilistic Approach for Evaluating Earthquake-Induced Landslides," Ph.D. Dissertation, Department of Civil, Architectural, and Environmental Engineering, University of Texas at Austin, Austin, TX.

Saygili, G. and Rathje, E.M. (2008) "Empirical Predictive Models for earthquake-Induced Sliding Displacements of Slopes," *Journal of Geotechnical and Geoenvironmental Engineering*, ASCE, 134(6), 790-803.

PUBLICATIONS RESULTING FROM THIS WORK

Saygili, G. (2008) *A Probabilistic Approach for Evaluating Earthquake-Induced Landslides*, Ph.D. Dissertation, Department of Civil, Architectural, and Environmental Engineering, University of Texas, Austin, TX.

Saygili, G. and Rathje, E.M. Submitted. "Probabilistically Based Seismic Landslide Hazard Maps," submitted for possible publication in *Engineering Geology*.